Synthesis of a novel nanocomposite based on date stones/CuFe₂O₄ nanoparticles for eliminating cationic and anionic dyes from aqueous solution

Noureddine El Messaoudi [a] *, Mohammed El Khomri [a], Abdelkader Dabagh [a],

Zahra Goodarzvand Chegini [b], Abdellah Dbik [a], Safae Bentahar [a], Abdellah Lacherai [a],

Munawar Iqbal [c], Amane Jada [d], Faroq Sher [e], Éder Cláudio Lima [f]

[a] *Laboratory of Applied Chemistry and Environment, Ibn Zohr University, Agadir 80000,*

Morocco

[b] *Science and Research Branch, Islamic Azad University, Tehran 99204, Iran*

[c] *Department of Chemistry, The University of Lahore, Lahore 53700, Pakistan*

[d] *Institute of Materials Science of Mulhouse (IS2M), High Alsace University, Mulhouse*

68100, France

[e] *Department of Engineering, School of Science and Technology, Nottingham Trent*

University, Nottingham NG11 8NS, United Kingdom

[f] *Institute of Chemistry, The Federal University of Rio Grande do Sul (UFRGS), Porto Alegre-*

RS 91501-970, Brazil

*Corresponding author. Tel.: +212675233867

E-mail address: noureddine.elmessaoudi@edu.uiz.ac.ma (N. El Messaoudi)

Abstract

In this study, the date stones/$CuFe_2O_4$ nanocomposite was synthesized by a graft of $CuFe_2O_4$ nanoparticles in the surface of date stones (DS) for the removal of rhodamine B (RhB) and methyl orange (MO) from aqueous solutions. The adsorption of RhB and MO on DS@$CuFe_2O_4$ shows good agreement with second-order kinetic and Langmuir isotherm models. The maximum adsorption capacity was found to be 555.56 03 mg g^{-1} and 303.03 mg g^{-1} for RhB and MO, respectively.This adsorption is spontaneous and endothermic. There is excellent regeneration and high reusability of the DS@$CuFe_2O_4$ for the RhB and MO removal in six cycles.

1. Introduction

Dyes are used in many industries such as textile, tannery, paper pulp, cosmetics, plastics, leather, printing, rubber, food, and pharmaceuticals [1–7]. The ingestion of dyes by human beings may cause cancer, mutagens, teratogens, cardiovascular shock, vomiting, gastrointestinal pain, diarrhoea, etc., and contamination of water with dyes causes serious problems for the environment and aquatic life [8–11]. Numerous studies have used many methods to remove dyes such as degradation, coagulation, photocatalysis, flocculation, hydrogen peroxide, adsorption, oxidation, irradiation, ion exchange, reverse osmosis, advanced oxidation, membrane filtration, precipitation, etc. [12–15]. Adsorption is a good technique because of its ease of operation, efficacy, high efficiency, and low energy demand. There are many adsorbents available and they are effective in regeneration and can be reused [16–23].

Agricultural solid wastes are lignocellulosic materials and their main components are cellulose, lignin, and hemicelluloses, lipids, proteins, etc. [16]. Agricultural wastes include

organic products, vegetables, fruits, meat, poultry, dairy items, and harvests. Agricultural solid wastes are extensively used to eliminate dyes from environmental wastewaters [24–27]. These materials are renewable and abundant in large quantities and have high potential as sorbents owing to the variety of functional groups (–OH, –C=O, –C–O, –NH$_2$) on their surface [28]. As a result, agricultural wastes can be used as an economic and eco-friendly adsorbent [29]. The date stone as agricultural solid waste used for dyes removal has been studied by others, but its performance as an adsorbent was limited because of its undeveloped porous structure [30–32].

Synthesizing approach and reaction parameters can have a significant influence on nanomaterial's magnetic, photocatalytic, and electrical properties [33, 34]. Nanostructures of CuFe$_2$O$_4$ have been developed by such reactions as solid-state [35, 36], sonochemical [37, 38], and hydrothermal [39, 40]. Besides, the ultrasonic-assisted approach is regarded as a simple, rapid, cost-effective, and eco-friendly method for creating nanostructured materials such as metals, metal chalcogenides, bimetal oxide, and graphene [41, 42].

In this work, DS@CuFe$_2$O$_4$ nanocomposite synthesized from date stones powder and CuFe$_2$O$_4$ nanoparticles were used for the removal of rhodamine and methyl orange from the aqueous solution. The synthesized nanocomposite was characterized by different analytical instruments such as Brunauer Emmett Teller (BET), Fourier transform infrared (FTIR), scanning electron microscope (SEM), and transition electron microscope (TEM) analysis. The research team investigated the influence of different experimental conditions through altering operational parameters such as initial pH of the solution, adsorbent dosage, contact time, pollutant concentration, and temperature. The RhB and MO adsorption on DS@CuFe$_2$O$_4$ were evaluated by kinetics (pseudo-first-order and pseudo-second-order) and equilibrium (Langmuir, Freundlich, and Temkin) models and thermodynamics parameters. The reusability of DS@CuFe$_2$O$_4$ nanocomposite was also investigated.

2. Experimental

2.1. Chemicals and reagents

Chemicals and reagents used in this study were as follows: Copper chloride dehydrate ($CuCl_2$, 2 H_2O), ferric chloride solution ($FeCl_3$, $4H_2O$), rhodamine B (cationic dye, $C_{28}H_{31}N_2O_3Cl$, CI=45170, MW=479.01 g mol^{-1}), methyl orange (anionic dye, $C_{14}H_{14}N_3NaO_3S$, CI=13025, MW=327.33 g mol^{-1}), deionized water, HCl, and NaOH. All chemicals were of analytical grade and purchased from Sigma-Aldrich.

2.2. Synthesis of CuFe$_2$O$_4$ nanoparticles

Copper chloride dihydrate ($CuCl_2$, 2 H_2O) was used as a precursor and was dissolved in deionized water, and then it was mixed drop by drop with ferric chloride solution ($FeCl_3.4H_2O$). Then, ultrasonic radiation with high intensity (100 W cm^{-2}), operating at 50 kHz, was used under ambient air for 1 h. The titanium horn was embedded to a depth of 4 cm in the solution. The reaction cell was not thermostated and the final temperature was 50 °C. After sonication, the solution was centrifuged at 5000 rpm for 4 min and rinsed with deionized water. Finally, one portion of the sample was over-dried (80 °C) for 12 h. The second portion of the sample was prepared by calcination in the furnace at 600 °C for 4 h.

2.3. Synthesis of DS@CuFe$_2$O$_4$ nanocomposite

Date stones (DS) were collected in Tinghir (South-East Morocco). The material was, crushed, sieved, and washed with ethanol and deionized water, then dried at 105 °C overnight. The DS@CuFe$_2$O$_4$ (date stones modified by CuFe$_2$O$_4$) nanocomposite was synthesized by addition of 1 g of date stones powder prepared and 2 g of CuFe$_2$O$_4$ nanoparticles in deionized water (1:2 v/v). The mixture was stirred for 3 h at room temperature. Then it was centrifuged, filtered, and dried in an oven for 16 h at 80 °C. After, the annealing process was conducted in a tube muffle furnace at 800 °C for 2 h to obtain the date stones nanoparticles (DS@CuFe$_2$O$_4$).

2.4. Characterization of adsorbent

96   The prepared adsorbent is characterized by various techniques. Brunauer Emmett Teller

97   (BET) model using Belsorp Mini II and Barrett-Joyner-Halenda (BJH) methods were employed

98   to evaluate the specific surface area and total pore volume, and diameter pore of

99   DS@CuFe$_2$O$_4$. Fourier transform infrared (FTIR) spectroscopy with resolution 4 cm^{-1} in a

100   spectrometer Jasco 4100 and coupled with attenuated total reflectance (ATR) technique in the

101   range 4000-400 cm^{-1} was used to determine the functional groups present in surface adsorbent.

102   Scanning electron microscope (SEM) on JEOL, JSM-IT200 at tension 20 kV and transition

103   electron microscope (TEM) using Philips CM-30 were used to specify the morphology of

104   DS@CuFe$_2$O$_4$.

105   **2.5. Removal of RhB and MO using DS@CuFe$_2$O$_4$**

106   The RhB and MO sorption were conducted in 250 mL Erlenmeyer flasks on a

107   thermostatic shaker in batch mode. A quantity of DS@CuFe$_2$O$_4$ was added to 50 mL of RhB or

108   MO dye solution (100 mg L^{-1}). The mixture was agitated at 170 rpm at 26 ± 1 °C for 50 min.

109   The influence of different parameters such as solution pH (3–11), DS@CuFe$_2$O$_4$ dosage (0.2–

110   1.2 g L^{-1}), contact time (0–120 min), initial dye concentration (50–400 mg L^{-1}), and

111   temperature (10–50 °C) on dyes adsorption was evaluated. The pH of the solution was adjusted

112   by 0.1 M HCl or 0.1 M sodium NaOH. The point of zero charge (PZC) value of DS@CuFe$_2$O$_4$

113   was determined using the method reported by Fiol and Villaescusa [43]. After completing the

114   experiment, the dye solution was filtered through centrifuging at 3500 rpm for 5 min. The

115   concentrations of residual RhB and MO were measured using a UV/Vis spectrophotometer

116   (2300/Techcomp) at 557 and 465 nm as λ_{max} of RhB and MO, respectively. The quantity

117   adsorbed q_e (mg g^{-1}) and removal efficiency (%) of RhB or MO onto DS@CuFe$_2$O$_4$ were

118   calculated by the equations given below:

119
$$q_e = \frac{(C_0 - C_e) \times V}{W} \qquad (1)$$

$$120 \qquad \% \, Removal = \frac{(C_0 - C_e)}{C_0} \times 100 \qquad (2)$$

121   Where, C_0 (mg L^{-1}) and C_e (mg L^{-1}) are the RhB or MO concentrations before and after

122   adsorption, respectively, V (L) is the dye solution volume and W (g) is the weight of

123   DS@CuFe$_2$O$_4$ used.

124   **3. Results and discussion**

125   **3.1. DS@CuFe$_2$O$_4$ characterization**

126   **3.1.1. BET and FTIR analysis**

127   Using the Brunauer Emmett Teller (BET) and Barrett-Joyner-Halenda (BJH) methods

128   **(Figure1a)**, the obtained average surface area was 52.16 m^2 g^{-1}, and the average pore diameter

129   was 17.34 nm and the total pore volume was 0.086 cm^3 g^{-1}.

130   Infrared spectroscopy helps us to a better comprehension of the functional group,

131   phase purity, and structural bonding between the metal and oxides in the nanocomposite. The

132   spectra FTIR of DS and DS@CuFe$_2$O$_4$ are shown in **Figure1b**. On the spectrum of DS, the

133   bond at 3435 cm^{-1} corresponds to hydroxyl −OH stretching vibration found on cellulose

134   hemicelluloses and lignin [44, 45]. The peak observed at 1747 cm^{-1} is attributed to stretching

135   vibration of –C=O owing to carboxyl group −COOH and may be assigned to carboxylic acids

136   of xylan in hemicelluloses [20, 46]. The peak at 1147 cm^{-1} is attributed to –C–O stretching

137   vibration of carboxylic acids and alcohols [47–49]. After modification of the DS with CuFe$_2$O$_4$

138   nanoparticles, we note the presence of the peaks at 586 cm^{-1} and 475 cm^{-1} corresponds to the

139   Fe and Cu [50–52], respectively. These peaks confirmed the complexation of CuFe$_2$O$_4$

140   nanoparticles with DS.

141

142
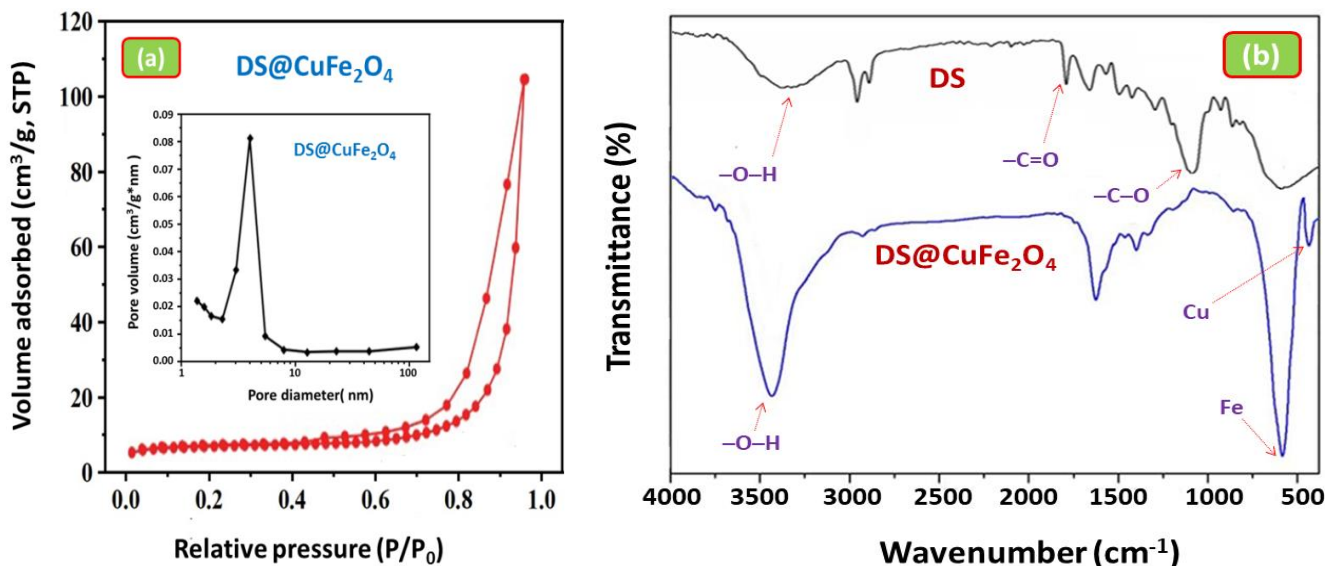
Figure1. Nitrogen adsorption/desorption isotherms included pore size of DS@CuFe$_2$O$_4$ (**a**) and FTIR spectra of DS and DS@CuFe$_2$O$_4$ (**b**).

3.1.2. SEM and TEM Analysis

To determine the quality of microstructures, the CuFe$_2$O$_4$ and DS@CuFe$_2$O$_4$ were examined by scanning electron microscope (SEM) and transition electron microscope (TEM). According to **Figure 2a, b**, the DS surface has different micropores in various shapes and sizes. **Figure 2c, d** shows CuFe$_2$O$_4$ surface and **Figure 2e, f** shows the development of DS surface micropores and also the dispersion of CuFe$_2$O$_4$ nanoparticles over it after modification.
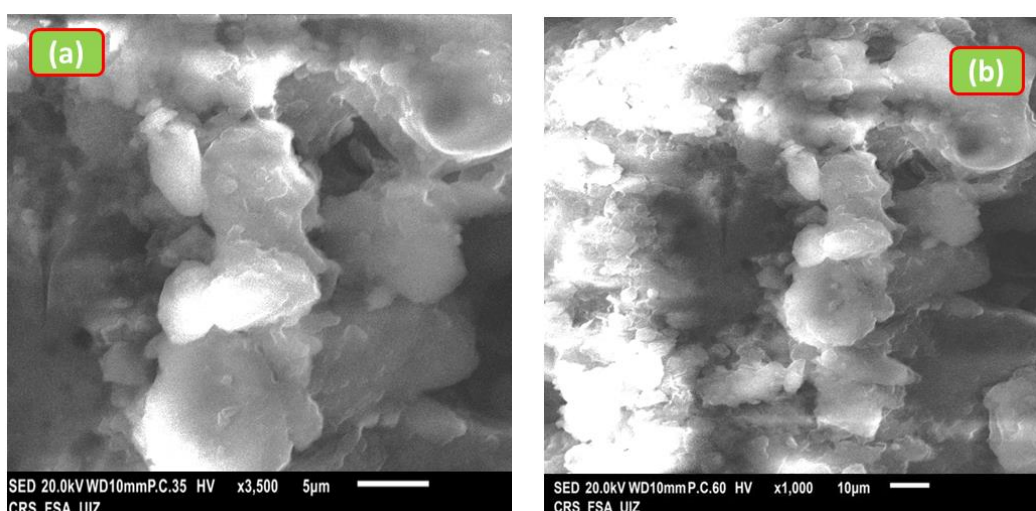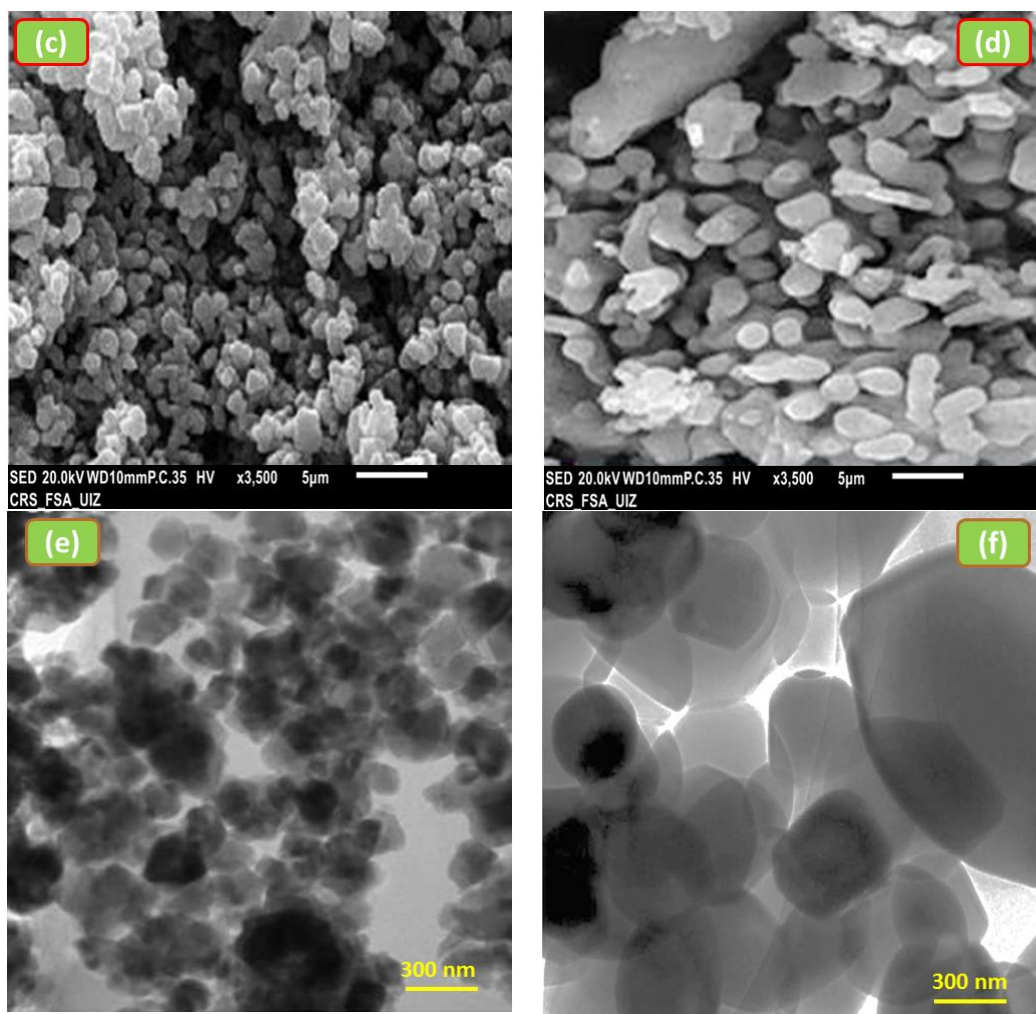
Figure2. SEM images of DS (**a,b**), CuFe$_2$O$_4$ (**c**), DS@CuFe$_2$O$_4$ (**d**), TEM imagesof CuFe$_2$O$_4$ (**e**), and DS@CuFe$_2$O$_4$ (**f**).

3.2. RhB and MO adsorption on DS@CuFe$_2$O$_4$

3.2.1. Effect of pH

To investigate the effect of initial solution pH on adsorption of RhB and MO in water, the batch experiments were conducted at different pH ranging from 3 to 11 (**Figure 3a**) at an initial concentration of 100 mg L^{-1} of dye, 0.2 g L^{-1} of adsorbent dosage and 120 min of contact time. The point of zero charge (PZC) is a crucial parameter to understand the adsorption process. As **Figure 3b** shows, pH$_{PZC}$ of DS@CuFe$_2$O$_4$ was 4.8. The highest removal efficiency was 84.65 % for RhB at pH=8 and 80.85 % for RhB at pH=5. As a result, the DS@CuFe$_2$O$_4$ surface charge will be positively charged at pH<pH$_{PZC}$ (adsorption of anionic

164 dye MO was favourable) and negatively charged when pH>pH$_{PZC}$ (adsorption of cationic dye

165 RhB was favourable) [53, 54].
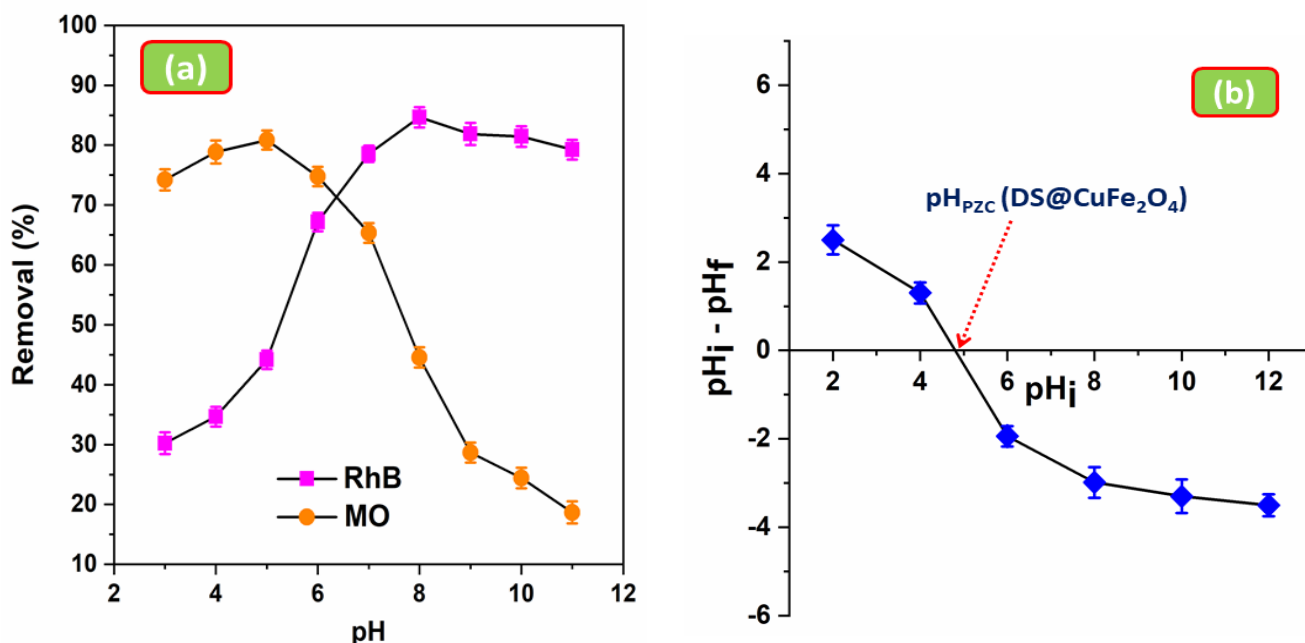
Figure3. Effect of pH on RhB and MO adsorption (**a**) and pH$_{PZC}$ of DS@CuFe$_2$O$_4$ (**b**).

167 **3.2.2. Effect of DS@CuFe$_2$O$_4$ dosage**

168 To evaluate the effect of DS@CuFe$_2$O$_4$ nanocomposite dosage, the adsorption

169 experiments were carried out with different dosages of 0.2 to 1.2 g L^{-1} whereas other

170 parameters were kept constant (RhB or MO concentration=100 mg L^{-1}, contact time =120

171 min, pH (RhB)=8, and pH (MO)=5). **Figure 4a** shows the results obtained. The RhB removal

172 increased from 64.66 to 97.84 % by increasing the adsorbent dosage from 0.2 to 0.4 g L^{-1}, and

173 the MO removal increased from 47.46 to 86.81 % by and from 0.2 to 0.6 g L^{-1}. Results imply

174 that the number of active adsorption sites for RhB and MO adsorption is corresponding to the

175 applied dose, which prompts higher removal efficiency [55]. After equilibrium between

176 the adsorbent and dye in the solution, the removal percentage remains consistent at higher

177 dosages (> 0.4 g L^{-1} for RhB and > 0.6 g L^{-1} for MO). The optimum adsorbent dosage was

178 considered 0.4 g L^{-1} RhB and 0.6 g L^{-1} to reach maximum RhB and MO removal efficiency,

179 respectively.

3.2.3. Effect of contact time

The contact time effect on adsorption of RhB and MO onto DS@CuFe$_2$O$_4$ was examined at an initial concentration of 100 mg L^{-1} of dye and 0.4 g L^{-1} and 0.6 g L^{-1} of adsorbent dosage for RhB and MO, respectively. As can be seen from **Figure 4b**, the RhB and MO adsorption was fast at first, but they declined after that. This may be attributed to many sites that are accessible on the surface of the nanocomposite in the initial stage [56]. With decreasing in several active sites, the adsorption rate became consistent [57]. Experimental data showed that equilibrium was achieved in 50 min with 244.40 mg g^{-1} and 159.72 mg g^{-1} adsorption capacity of RhB and MO, respectively.

3.2.4. Effect of initial dye concentration

As a function of initial RhB and MO concentrations, two factors of removal efficiency and equilibrium adsorption capacities were investigated. The initial RhB and MO concentrations varied from 50 to 400 mg L^{-1} with keeping all other parameters consistent (DS@CuFe$_2$O$_4$ dosage: 0.4 g L^{-1} (RhB): 0.6 g L^{-1} (MO), temperature: 26 ± 1 °C, contact time: 50 min, pH (RhB) = 8, and pH (MO) = 5. The results are depicted in **Figure 4c**. As illustrated in **Figure 4c**, by increasing RhB and MO concentrations, adsorption capacity progressively increased owing to the occupation of all available sites on the surface of nanocomposite by RhB and MO molecules. But, a plateau was not achieved in the adsorption capacity, suggesting active sites are still available and no saturation occurred [58]. On the other hand, removal efficiency decreased because of increasing the competition among RhB and MO molecules for occupying available sites. Dye initial concentration is an important factor in the adsorption process because as a driving force, it overcomes the resistance of mass transfer between solution and solid phases [59].
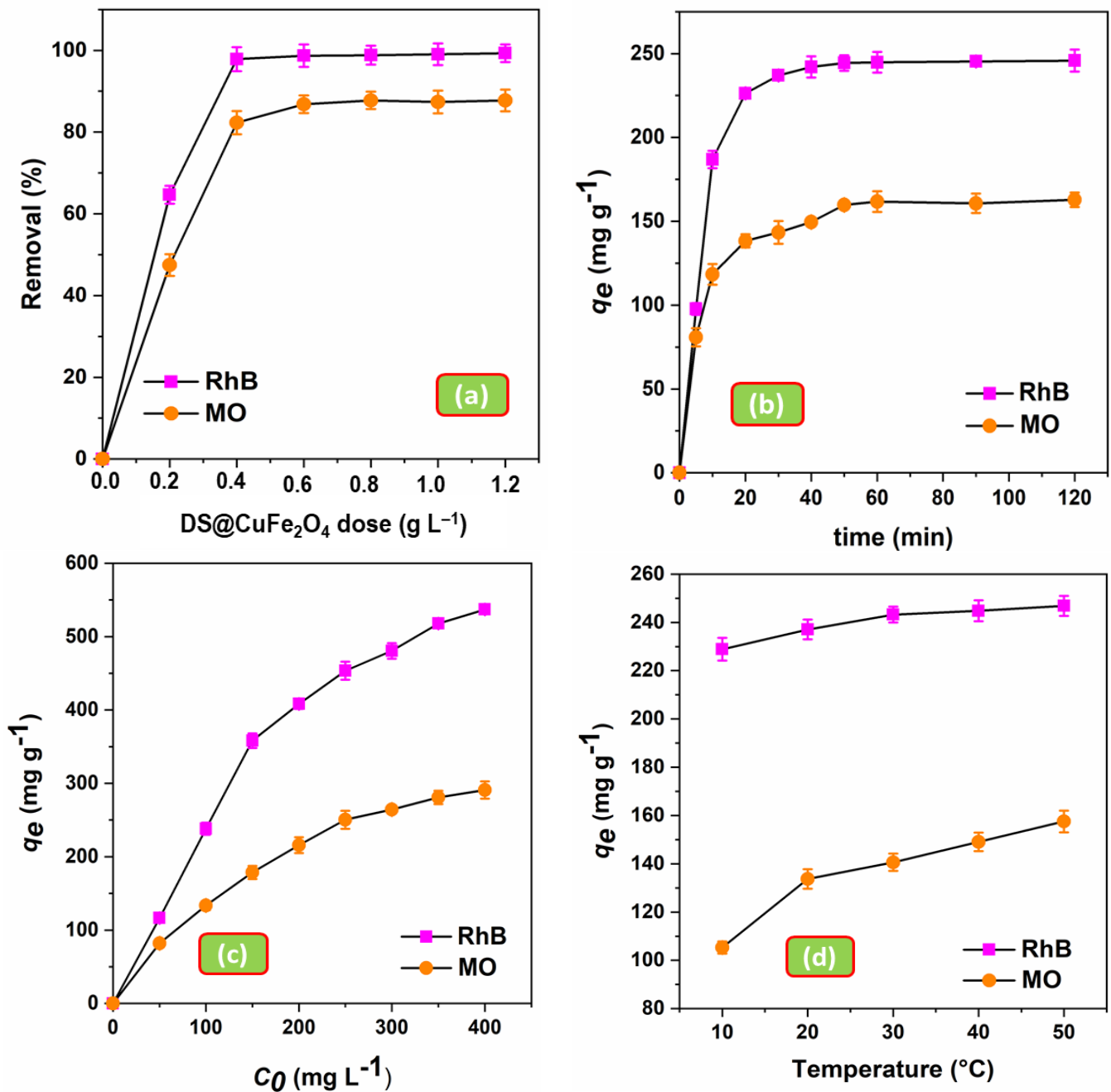
Figure 4. Percentage of RhB and MO removal as a function DS@CuFe$_2$O$_4$ dosage (**a**), Effects of contact time (**b**), initial dye concentration (**c**), and temperature (**d**) on RhB and MO adsorption using DS@CuFe$_2$O$_4$.

3.2.5. Effect of temperature

Figure 4d shows the RhB and MO adsorption on DS@CuFe$_2$O$_4$ using 50 mL of 100 mg L^{-1} dye solution at different temperatures (10, 20, 30, 40, and 50 °C). It was seen that temperature was increased from 10 to 50 °C for adsorption capacity of dye increased from

213   228.86 to 246.84 mg g^{-1} for RhB and from 105.30 to 157.51 mg g^{-1} for MO at 50 min of contact

214   time and pH=8 for RhB and pH=5 for MO. This increase was because the mobility accelerated

215   of dye molecules with increasing of temperature and therefore the sites at the surface of

216   adsorbent were active, and the adsorption is an endothermic reaction [59].

217   **3.3. Adsorption modeling**

218   **3.3.1. Kinetic examination**

219   The RhB and MO adsorption on DS@CuFe$_2$O$_4$ was evaluated using two kinetic (pseudo-

220   first-order and pseudo-second-order) models and are expressed by the equations below [60–

221   62]:

$$Log(q_e - q_t) = Log(q_e) - \frac{K_1}{2.303}t \qquad (3)$$

$$\frac{t}{q_t} = \frac{1}{K_2 q_e{}^2} + \frac{1}{q_e}t \qquad (4)$$

224   Where, q_t, (mg g^{-1}) and q_e, (mg g^{-1}) are the amounts adsorbed at t and equilibrium,

225   respectively, t is the time of reaction, K_1 (min^{-1}) and K_2 (g mg^{-1} min^{-1}) are the constants related

226   to the first-order and second-order, respectively. **Figure 5** shows the kinetic adsorption curves

227   plotted for the two kinetic models. **Table 1** shows the parameters for linear fitting. The

228   experimental data observed fit with the second-order model. It can be found that the correlation

229   coefficients r^2 are very near to 1 for the two dyes. The experimental $q_{e,exp}$ values are also closer

230   to the theoretically calculated $q_{e,\ cal}$ values for the second-order model. These results

231   demonstrated that RhB and MO adsorption on DS@CuFe$_2$O$_4$ follows a second-order kinetic

232   model.

233   The optimization procedure requires an error function for evaluating the fit of the equation

234   to the experimental data. The residual root means square error (*RMSE*) and the sum of squares

235   error (*SSE*) is calculated from the following Eqs. (5) and (6), respectively [63, 64]:

$$RMSE = \sqrt{\sum_{i=1}^{N} \frac{(q_{e,exp} - q_{e,cal})^2 \, i}{N}} \qquad (5)$$

$$SSE = \sum_{i=1}^{N} (q_{e,exp} - q_{e,cal})^2 \, i \qquad (6)$$

$N=$ Number of experimental points.
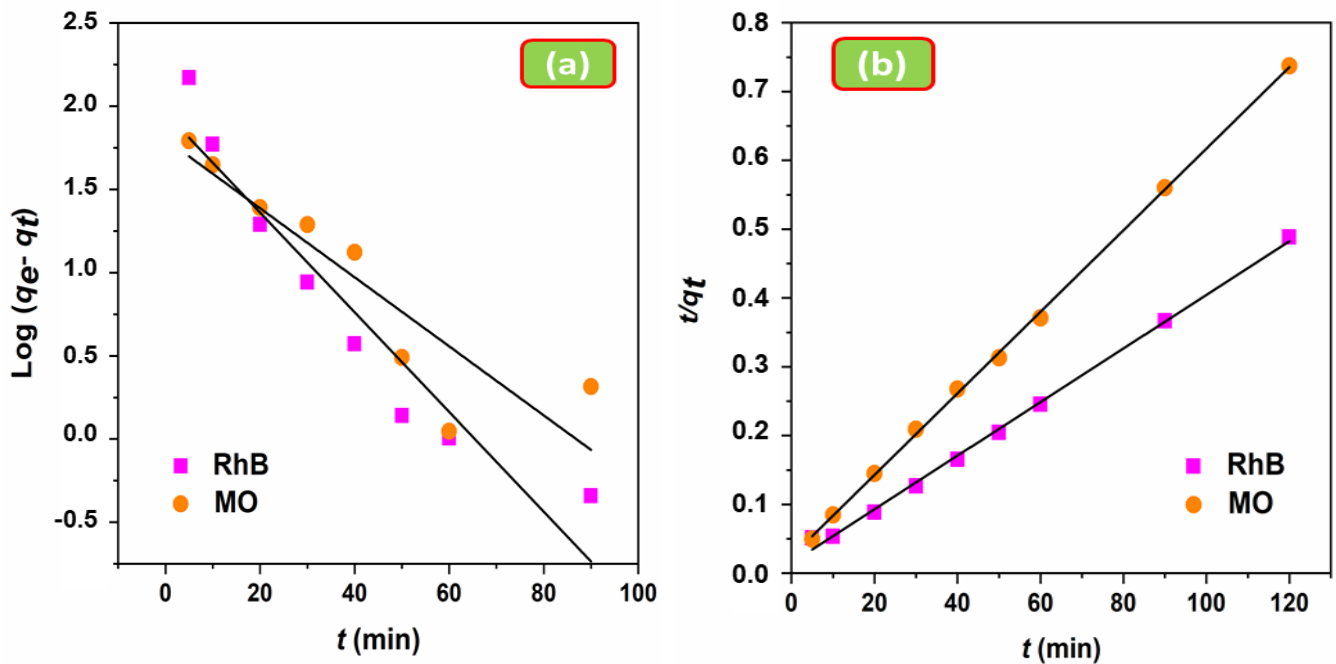
Figure 5. Kinetic curves of RhB and MO adsorption on DS@CuFe$_2$O$_4$: pseudo-first-order (**a**) and pseudo-second-order (**b**) models.

Table 1. Kinetic model parameters for RhB and MO adsorption on DS@CuFe$_2$O$_4$.

Model	Parameter	RhB	MO
Pseudo-first-order	$q_{e,,exp}$ (mg g^{-1})	245.79	162.81
	K_1 (min^{-1})	0.069	0.047
	$q_{e,\,cal}$ (mg g^{-1})	91.28	63.40
	r^2	0.912	0.820
	RMSE	1.016	2.326
	SEE	4.347	3.192
Pseudo-second-order	K_2 (g mg^{-1} min^{-1})	0.001	0.002
	$q_{e,\,cal}$ (mg g^{-1})	256.41	169.49
	r^2	0.997	0.999
	RMSE	0.945	2.072
	SEE	3.026	2.438

3.3.2. Equilibrium investigation

The correlation between adsorption capacity and dye concentration in a liquid phase at equilibrium was determined using Langmuir, Freundlich, and Temkin isotherm models and is represented by the equations below, respectively [65–67]:

$$\frac{C_e}{q_e} = \frac{1}{Q_m K_L} + \frac{C_e}{Q_m} \qquad (7)$$

$$Ln q_e = Ln K_F + \frac{Ln C_e}{n} \qquad (8)$$

$$q_e = B Ln K_T + B Ln C_e \qquad (9)$$

Where, Q_m (mg g^{-1}) is the maximum dye per gram of adsorbent, K_L (L mg^{-1}) is the constant of Langmuir isotherm, K_F ((mg g^{-1})(L mg^{-1})$^{1/n}$) is the constant related to Freundlich isotherm, K_T (L g^{-1}) is the constant of Temkin isotherm and B is the constant related to the heat adsorption. The results obtained are shown in **Figure 6** and the calculated parameters are given in **Table 2**. Based on correlation coefficient r^2, the Langmuir model best described the RhB and MO adsorption equilibrium data. Langmuir model suggests the dye adsorption occurs as a monolayer from the homogeneous surface of the adsorbent [68]. A similar observation was found in other studies, which also have shown the successful prediction of adsorption isotherm data using Langmuir isotherm as compared to Freundlich and Temkin isotherm models [69–72].
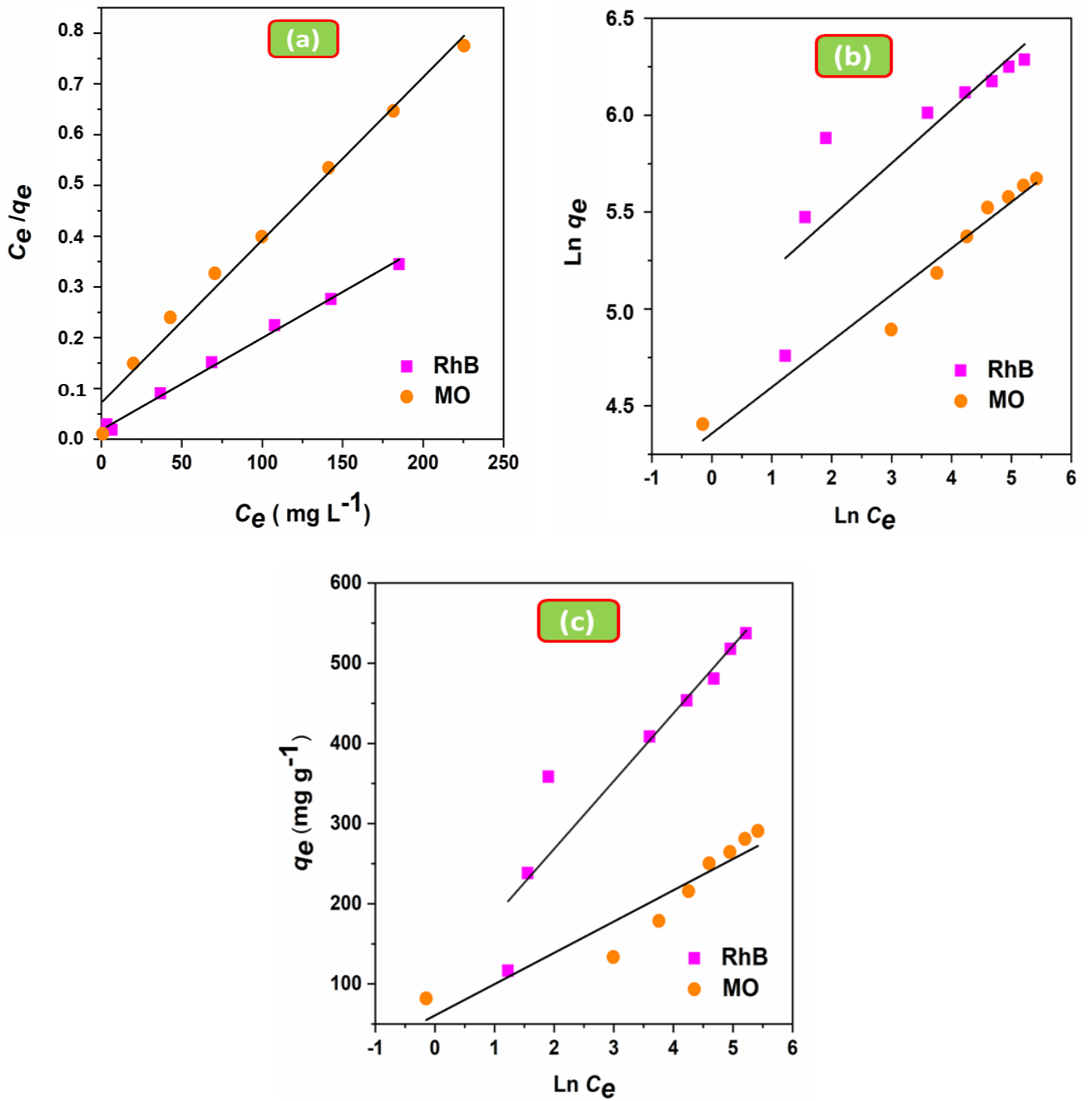
Figure 6. Equilibrium curves of RhB and MO adsorption on DS@CuFe$_2$O$_4$:
Langmuir (**a**), Freundlich (**b**), and Temkin (**c**) isotherm models.

Table 2. Isotherm model parameters for RhB and MO adsorption on DS@CuFe$_2$O$_4$.

Model	Parameter	RhB	MO
	Q_m (mg g^{-1})	555.56	303.03
Langmuir	K_L (L mg^{-1})	0.097	0.057
	r^2	0.995	0.993
	K_F ((mg g^{-1}) (L mg^{-1})$^{1/n}$)	137.414	84.040
Freundlich	N	3.617	4.385
	r^2	0.748	0.922
	K_T (L g^{-1})	3.246	6.472
Temkin	B	84.503	37.670
	r^2	0.883	0.938

3.3.3. Thermodynamic analysis

The thermodynamic parameters of RhB and MO adsorption on DS@CuFe$_2$O$_4$ such as the free energy $\Delta G°$, the enthalpy $\Delta H°$, and the s entropy $\Delta S°$ were calculated by the equations below [73, 74]:

$$\Delta G° = -RTLnK_C \qquad (10)$$

$$LnK_C = \frac{\Delta S°}{R} - \frac{\Delta H°}{RT} \qquad (11)$$

Where, R (8.314 J mol^{-1} K^{-1}) is the constant of perfect gases, T (K) is the absolute temperature and K_C is the equilibrium constant, $\Delta H°$ was obtained from the slope of LnK_C versus $1/T$ (K^{-1}) and $\Delta S°$ was obtained from y-intercept for adsorption of dye. **Table 3** shows the thermodynamic adsorption parameters of RhB and MO on DS@CuFe$_2$O$_4$.. The negative value of $\Delta G°$ at five temperatures suggested the feasibility and spontaneity of the RhB and MO adsorption on DS@CuFe$_2$O$_4$. This adsorption is physical because the $\Delta G°$ was lower than 0 kJ mol^{-1} [75]. The positive $\Delta H°$ values verified the endothermic nature of the adsorption process [46, 76]. The positive $\Delta S°$ values indicate that the disorder increases at the adsorbent/solution interface [77, 78].

292   **Table 3**. Thermodynamic parameters for RhB and MO adsorption on DS@CuFe$_2$O$_4$.

Dye	T (K)	$\Delta G°$ (kJ mol^{-1})	$\Delta H°$ (kJ mol^{-1})	$\Delta S°$ (J mol^{-1} K^{-1})
RhB	283	−06.394		
	293	−07.804		
	303	−09.615	37.713	153.044
	313	−10.327		
	323	−11.702		
MO	283	−01.315		
	293	−03.412		
	303	−04.106	40.931	149.610
	313	−05.203		
	323	−06.929		

293

3.4. Comparison with other adsorbents

295   The maximum adsorption capacity of DS@CuFe$_2$O$_4$ for RhB and MO was compared

296   with the previous study; see **Table 4**. The results show that DS@CuFe$_2$O$_4$ has good adsorption

297   performance on the RhB and MO removal, better than some adsorbents previously reported in

298   the literature.

299   **Table 4**. Comparison of adsorption capacity of RhB and MO with previous studies.

| Adsorbent	Q_m (mg g^{-1})		Refs.
	RhB	**MO**	
Magnetic pectin/ *Chlorella vulgaris*	–	109.11	[79]
Ghum ghati/Fe$_3$O$_4$	529.10	–	[69]
α-MnO$_2$ nanoparticles	–	116.10	[72]
Magnetic activated carbon/CeO$_2$	324.60	–	[80]
ZnO/Zr-MOF(bpy)	918.90	–	[81]
Graphene boron nitride/SiO$_2$	625.00	–	[70]
Fe$_3$O$_4$/C	87.32	38.03	[82]
Graphene oxide/carbon nanotube	248.48	66.96	[83]
Bentonite/ carbon nanotube	148.20	–	[71]
PANi-BiVO$_4$	–	75.90	[84]
Biobased magnetic hollow particles	50.40	–	[85]
Functionalized-CNTs loaded TiO$_2$	42.85	–	[86]
DS@CuFe$_2$O$_4$	555.56	303.03	This study

300

301

302

303

304   **3.5. Reusability of DS@CuFe₂O₄**

305   After adsorption of dye, the DS@CuFe$_2$O$_4$ was regenerated by washing many times

306   with 0.01 M HCl and 0.01M NaOH for their reusability in the RhB and MO removal from

307   aqueous solution, respectively; see the results in **Figure7**. It is noted that adsorption efficiency

308   decreases from 98.54 to 83.15 % for RhB and from 95.22 to 79.08 % for MO after six cycles.

309   This decrease was attributed to the occupation of available sites on the DS@CuFe$_2$O$_4$ surface

310   [87]. The above result further indicated the DS@CuFe$_2$O$_4$ could be reused for the removal of

311   organic dyes in wastewater.
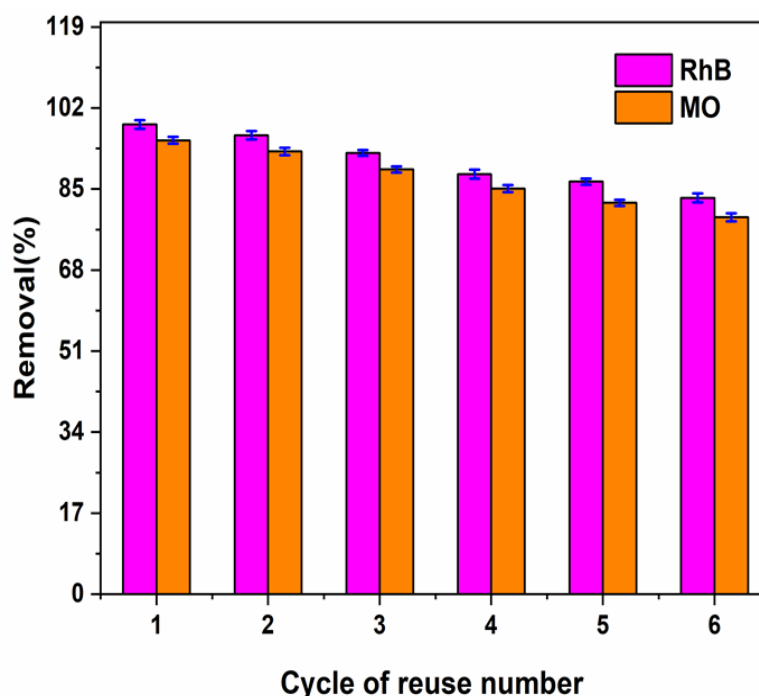
312

313   **Figure 7**. Reusability of DS@CuFe$_2$O$_4$ in the removal of RhB and MO dyes.

4. Conclusion

        In this study, a novel nanocomposite was synthesized with date stones modified by

CuFe$_2$O$_4$ and it was applied for rhodamine B and methyl orange removal from aqueous

solutions. The results of the adsorption experiment conducted in batch mode revealed

optimum conditions for RhB and MO adsorption by DS@CuFe$_2$O$_4$ nanocomposite. Dye

removal was maximum at pH=8 for RhB and pH=5 for and RhB and equilibrium were achieved

in 50 min. The result of FTIR, SEM, and TEM characterization verified the dispersion and complexation of $CuFe_2O_4$ nanoparticles with DS. Kinetic and isotherm models were fitted to the experimental data, showing that pseudo-second-order kinetic and Langmuir isotherm models were best fitted to the data. The maximum adsorption capacity was 555.56 and 303.03 mg g^{-1} for RhB and MO, respectively. The thermodynamic study revealed that physisorption is the dominant mechanism and adsorption of RhB and MO to nanocomposite is endothermic. The finding suggested that DS@$CuFe_2O_4$ nanocomposite could be considered as an efficient adsorbent to remove dyes from aqueous solutions.

317 **Disclosure Statement**

318 No potential conflict of interest was reported by the authors.

319

References

[1]   Zhou, Y., Lu, J., Zhou, Y., & Liu, Y., 2019, Recent advances for dyes removal using novel adsorbents: A review. *Environmental Pollution* **252**, 352–365. https://doi.org/10.1016/J.ENVPOL.2019.05.072

[2]   González, J. A., Villanueva, M. E., Piehl, L. L., & Copello, G. J., 2015, Development of a chitin/graphene oxide hybrid composite for the removal of pollutant dyes: Adsorption and desorption study. *Chemical Engineering Journal* **280**, 41–48. https://doi.org/10.1016/j.cej.2015.05.112

[3]   Ip, A. W. M., Barford, J. P., & McKay, G., 2009, Reactive Black dye adsorption/desorption onto different adsorbents: Effect of salt, surface chemistry, pore size and surface area. *Journal of Colloid and Interface Science* **337**, 32–38. https://doi.org/10.1016/j.jcis.2009.05.015

[4]   Mittal, A., Mittal, J., Malviya, A., & Gupta, V. K., 2009, Adsorptive removal of hazardous anionic dye "Congo red" from wastewater using waste materials and recovery by desorption. *Journal of Colloid and Interface Science* **340**, 16–26. https://doi.org/10.1016/j.jcis.2009.08.019

[5]   El Messaoudi, N., El Khomri, M., Dbik, A., Bentahar, S., Lacherai, A., & Bakiz, B., 2016, Biosorption of Congo red in a fixed-bed column from aqueous solution using jujube shell: Experimental and mathematical modeling. *Journal of Environmental Chemical Engineering* **4**, 3848–3855. https://doi.org/10.1016/j.jece.2016.08.027

[6]   Bayazıt, G., Gül, Ü. D., & Ünal, D., 2019, Biosorption of Acid Red P-2BX by lichens as low-cost biosorbents. *International Journal of Environmental Studies* **76**, 608–615. https://doi.org/10.1080/00207233.2018.1502959

[7]   Mohan, D., Singh, V. N., Kaul, S. N., & Sharma, Y. C., 2002, Removal of Lissamine Red from wastewater using waste materials. *International Journal of Environmental*

345   *Studies* **59**, 115–124. https://doi.org/10.1080/00207230211960

346 [8] El Messaoudi, N., El Khomri, M., Chlif, N., Chegini, Z. G., Dbik, A., Bentahar, S., &

347   Lacherai, A., 2021, Desorption of Congo red from dye-loaded Phoenix dactylifera date

348   stones and Ziziphus lotus jujube shells. *Groundwater for Sustainable Development* **12**,

349   100552. https://doi.org/10.1016/j.gsd.2021.100552

350 [9] Afroze, S., Sen, T. K., Ang, M., & Nishioka, H. ,2016, Adsorption of methylene blue

351   dye from aqueous solution by novel biomass Eucalyptus sheathiana bark: equilibrium,

352   kinetics, thermodynamics and mechanism.*Desalination and Water Treatment* **57**,

353   5858–5878. https://doi.org/10.1080/19443994.2015.1004115

354 [10] Azzaz, A. A., Jellali, S., Assadi, A. A., & Bousselmi, L., 2016, Chemical treatment of

355   orange tree sawdust for a cationic dye enhancement removal from aqueous solutions:

356   kinetic, equilibrium and thermodynamic studies. *Desalination and Water Treatment* **57**,

357   22107–22119. https://doi.org/10.1080/19443994.2015.1103313

358 [11] El Messaoudi, N., El Khomri, M., Goodarzvand Chegini, Z., Chlif, N., Dbik, A.,

359   Bentahar, S., Lacherai, A., 2021, Desorption study and reusability of raw and H $_2$ SO $_4$

360   modified jujube shells (*Zizyphus lotus*) for the methylene blue adsorption.

361   *International Journal of Environmental Analytical Chemistry*.

362   https://doi.org/10.1080/03067319.2021.1912338

363 [12] Chandane, V., & Singh, V. K., 2016, Adsorption of safranin dye from aqueous

364   solutions using a low-cost agro-waste material soybean hull. *Desalination and Water*

365   *Treatment* **57**, 4122–4134. https://doi.org/10.1080/19443994.2014.991758

366 [13] Sadaf, S., & Bhatti, H. N., 2016, Response surface methodology approach for

367   optimization of adsorption process for the removal of Indosol Yellow BG dye from

368   aqueous solution by agricultural waste. *Desalination and Water Treatment* **57**, 11773–

369   11781. https://doi.org/10.1080/19443994.2015.1048308

370 [14] Akpomie, K. G., & Conradie, J., 2020, Banana peel as a biosorbent for the

371 decontamination of water pollutants. A review. *Environmental Chemistry Letters* **18**,

372 1085–1112. https://doi.org/10.1007/s10311-020-00995-x

373 [15] Bentahar, S., Dbik, A., Khomri, M. E., El Messaoudi, N., & Lacherai, A., 2017,

374 Adsorption of methylene blue, crystal violet and congo red from binary and ternary

375 systems with natural clay: Kinetic, isotherm, and thermodynamic. *Journal of*

376 *Environmental Chemical Engineering* **5**, 5921–5932.

377 https://doi.org/10.1016/j.jece.2017.11.003

378 [16] Bhatnagar, A., Sillanpää, M., & Witek-Krowiak, A. ,2015, Agricultural waste peels as

379 versatile biomass for water purification - A review. *Chemical Engineering Journal* **270**,

380 244–271. https://doi.org/10.1016/j.cej.2015.01.135

381 [17] Ali, I., Asim, M., & Khan, T. A., 2012, Low cost adsorbents for the removal of organic

382 pollutants from wastewater. *Journal of Environmental Management* **113**, 170–183

383 https://doi.org/10.1016/j.jenvman.2012.08.028

384 [18] Bayram, T., Bucak, S., & Ozturk, D., 2020, BR13 dye removal using sodium dodecyl

385 sulfate modified montmorillonite: Equilibrium, thermodynamic, kinetic and reusability

386 studies. *Chemical Engineering and Processing - Process Intensification* **158**, 108186.

387 https://doi.org/10.1016/j.cep.2020.108186

388 [19] Wang, Q., Lei, L., Wang, F., Chen, C., Kang, X., Wang, C., Chen, Z., 2020,

389 Preparation of egg white@zeolitic imidazolate framework-8@polyacrylic acid aerogel

390 and its adsorption properties for organic dyes. *Journal of Solid State Chemistry* **292**,

391 121656. https://doi.org/10.1016/j.jssc.2020.121656

392 [20] El Messaoudi, N., El Khomri, M., Bentahar, S., Dbik, A., Lacherai, A., & Bakiz, B.,

393 2016, Evaluation of performance of chemically treated date stones: Application for the

394 removal of cationic dyes from aqueous solutions. *Journal of the Taiwan Institute of*

395   *Chemical Engineers* **67**, 244–253. https://doi.org/10.1016/j.jtice.2016.07.024

396   [21]   Mehralian, M., Goodarzvand Chegini, Z., & Khashij, M., 2019, Activated carbon

397   prepared from pistachio waste for dye adsorption: experimental and CCD-based design.

398   *Pigment and Resin Technology* **49**, 136–144. https://doi.org/10.1108/PRT-06-2019-

399   0052

400   [22]   Lakshmipathy, R., & Sarada, N. C., 2014, Adsorptive removal of basic cationic dyes

401   from aqueous solution by chemically protonated watermelon (Citrullus lanatus) rind

402   biomass. *Desalination and Water Treatment* **52**, 6175–6184.

403   https://doi.org/10.1080/19443994.2013.812526

404   [23]   Lafi, R., Hamdi, N., & Hafiane, A., 2015, Study of the performance of Esparto grass

405   fibers as adsorbent of dyes from aqueous solutions. *Desalination and Water Treatment*

406   **56**, 722–735. https://doi.org/10.1080/19443994.2014.950993

407   [24]   Bharathi, K. S., & Ramesh, S. T., 2013, Removal of dyes using agricultural waste as

408   low-cost adsorbents: a review. *Applied Water Science* **3**, 773–790.

409   https://doi.org/10.1007/s13201-013-0117-y

410   [25]   Afroze, S., & Sen, T. K., 2018, A Review on Heavy Metal Ions and Dye Adsorption

411   from Water by Agricultural Solid Waste Adsorbents. *Water, Air, and Soil Pollution*

412   **229**, 1–50. https://doi.org/10.1007/s11270-018-3869-z

413   [26]   Chong, M. Y., & Tam, Y. J., 2020, Bioremediation of dyes using coconut parts via

414   adsorption: a review. *SN Applied Sciences* **2**, 1–16. https://doi.org/10.1007/s42452-

415   020-1978-y

416   [27]   Dbik, A., Bentahar, S., El Khomri, M., El Messaoudi, N., & Lacherai, A., 2020,

417   Adsorption of Congo red dye from aqueous solutions using tunics of the corm of the

418   saffron. In *Materials Today: Proceedings* **22**, 134–139.

419   https://doi.org/10.1016/j.matpr.2019.08.148

420   [28]   Ghorbani, F., Kamari, S., Zamani, S., Akbari, S., & Salehi, M., 2020, Optimization and

421   modeling of aqueous Cr(VI) adsorption onto activated carbon prepared from sugar beet

422   bagasse agricultural waste by application of response surface methodology. *Surfaces*

423   *and Interfaces* **18**, 100444. https://doi.org/10.1016/j.surfin.2020.100444

424   [29]   Saka, C., Şahin, Ö., & Küçük, M. M., 2012, Applications on agricultural and forest

425   waste adsorbents for the removal of lead (II) from contaminated waters. *International*

426   *Journal of Environmental Science and Technology* **9**, 379–394.

427   https://doi.org/10.1007/s13762-012-0041-y

428   [30]   Abbas, A. F., & Ahmed, M. J., 2016, Mesoporous activated carbon from date stones

429   (Phoenix dactylifera L.) by one-step microwave assisted K_2CO_3 pyrolysis. *Journal of*

430   *Water Process Engineering* **9**, 201–207. https://doi.org/10.1016/j.jwpe.2016.01.004

431   [31]   Wakkel, M., Khiari, B., & Zagrouba, F., 2019, Textile wastewater treatment by agro-

432   industrial waste: Equilibrium modelling, thermodynamics and mass transfer

433   mechanisms of cationic dyes adsorption onto low-cost lignocellulosic adsorbent.

434   *Journal of the Taiwan Institute of Chemical Engineers* **96**, 439–452.

435   https://doi.org/10.1016/j.jtice.2018.12.014

436   [32]   Arunachalam, A., Chaudhuri, R. G., Iype, E., & Prakash Kumar, B. G., 2018, Surface

437   modification of date seeds (Phoenix dactylifera) using potassium hydroxide for

438   wastewater treatment to remove azo dye. *Water Practice and Technology* **13**, 859–870.

439   https://doi.org/10.2166/wpt.2018.095

440   [33]   Astaraki, H., Masoudpanah, S. M., & Alamolhoda, S., 2020, Effects of fuel contents on

441   physicochemical properties and photocatalytic activity of $CuFe_2O_4$/reduced graphene

442   oxide (RGO) nanocomposites synthesized by solution combustion method. *Journal of*

443   *Materials Research and Technology* **9**, 13402–13410.

444   https://doi.org/10.1016/j.jmrt.2020.09.072

445   [34]   Zhao, Y., Lin, C., Bi, H., Liu, Y., & Yan, Q., 2017, Magnetically separable $CuFe_2O_4$

446   /AgBr composite photocatalysts: Preparation, characterization, photocatalytic activity

447   and photocatalytic mechanism under visible light. *Applied Surface Science* **392**, 701–

448   707. https://doi.org/10.1016/j.apsusc.2016.09.099

449   [35]   Xing, Z., Ju, Z., Yang, J., Xu, H., & Qian, Y., 2013, One-step solid state reaction to

450   selectively fabricate cubic and tetragonal $CuFe_2O_4$ anode material for high power

451   lithium ion batteries. *Electrochimica Acta* **102**, 51–57.

452   https://doi.org/10.1016/j.electacta.2013.03.174

453   [36]   Sun, Z., Liu, L., Jia, D. zeng, & Pan, W., 2007,Simple synthesis of CuFe2O4

454   nanoparticles as gas-sensing materials. *Sensors and Actuators, B: Chemical* **125**, 144–

455   148. https://doi.org/10.1016/j.snb.2007.01.050

456   [37]   Amulya, M. A. S., Nagaswarupa, H. P., Kumar, M. R. A., Ravikumar, C. R., Kusuma,

457   K. B., & Prashantha, S. C., 2021, Evaluation of bifunctional applications of $CuFe_2O_4$

458   nanoparticles synthesized by a sonochemical method. *Journal of Physics and*

459   *Chemistry of Solids* **148**, 109756. https://doi.org/10.1016/j.jpcs.2020.109756

460   [38]   Mondal, B., Kundu, M., Mandal, S. P., Saha, R., Roy, U. K., Roychowdhury, A., &

461   Das, D., 2019, Sonochemically Synthesized Spin-Canted $CuFe_2O_4$ Nanoparticles for

462   Heterogeneous Green Catalytic Click Chemistry. *ACS Omega* **4**, 13845–13852.

463   https://doi.org/10.1021/acsomega.9b01477

464   [39]   Phuruangrat, A., Kuntalue, B., Thongtem, S., & Thongtem, T., 2016, Synthesis of

465   cubic $CuFe_2O_4$ nanoparticles by microwave-hydrothermal method and their magnetic

466   properties. *Materials Letters* **167**, 65–68. https://doi.org/10.1016/j.matlet.2016.01.005

467   [40]   Hou, H., Xu, G., Tan, S., & Xiang, S., 2018, A facile hydrothermal synthesis of

468   nanoscale $CuFe_2O_4$ spinels with enhanced infrared radiation performance. *Journal of*

469   *Alloys and Compounds* **735**, 2205–2211. https://doi.org/10.1016/j.jallcom.2017.11.370

470   [41]   Meigoli Boushehrian, M., Esmaeili, H., & Foroutan, R., 2020,Ultrasonic assisted

471   synthesis of Kaolin/CuFe2O4nanocomposite for removing cationic dyes from aqueous

472   media. *Journal of Environmental Chemical Engineering* **8**, 103869.

473   https://doi.org/10.1016/j.jece.2020.103869

474   [42]   Janani, B., Syed, A., Thomas, A. M., Al-Rashed, S., Raju, L. L., & Khan, S. S., 2020,

475   A simple approach for the synthesis of bi-functional p-n type $ZnO@CuFe_2O_4$

476   heterojunction nanocomposite for photocatalytic and antimicrobial application. *Physica*

477   *E: Low-dimensional Systems and Nanostructures* **130**, 114664.

478   https://doi.org/10.1016/j.physe.2021.114664

479   [43]   Fiol, N., & Villaescusa, I., 2009, Determination of sorbent point zero charge:

480   Usefulness in sorption studies. *Environmental Chemistry Letters* **7**,79–84.

481   https://doi.org/10.1007/s10311-008-0139-0

482   [44]   Salomón, Y. L. d. O., Georgin, J., Franco, D. S. P., Netto, M. S., Grassi, P., Piccilli, D.

483   G. A.,Dotto, G. L., 2020, Powdered biosorbent from pecan pericarp (Carya illinoensis)

484   as an efficient material to uptake methyl violet 2B from effluents in batch and column

485   operations. *Advanced Powder Technology* **31**, 2843–2852.

486   https://doi.org/10.1016/j.apt.2020.05.004

487   [45]   Shakoor, S., & Nasar, A., 2019, Utilization of Cucumis Sativus Peel as an Eco-Friendly

488   Biosorbent for the Confiscation of Crystal Violet Dye from Artificially Contaminated

489   Wastewater . *Analytical Chemistry Letters* **9**, 1–19.

490   https://doi.org/10.1080/22297928.2019.1588162

491   [46]   Guo, H., Yan, L., Song, D., & Li, K., 2016, Citric acid modified Camellia oleifera shell

492   for removal of crystal violet and Pb(II): parameters study and kinetic and

493   thermodynamic profile. *Desalination and Water Treatment* **57**, 15373–15383.

494   https://doi.org/10.1080/19443994.2015.1072057

495   [47]   Feng, N. C., & Guo, X. Y., 2012, Characterization of adsorptive capacity and

496   mechanisms on adsorption of copper, lead and zinc by modified orange peel.

497   *Transactions of Nonferrous Metals Society of China* **22**, 1224–1231.

498   https://doi.org/10.1016/S1003-6326(11)61309-5

499   [48]   Singh, J., Ali, A., Jaswal, V. S., & Prakash, V., 2015, Desalination of Cd^{2+} and Pb^{2+}

500   from paint industrial wastewater by Aspergillus niger decomposed Citrus limetta peel

501   powder. *International Journal of Environmental Science and Technology* **12**, 2523–

502   2532. https://doi.org/10.1007/s13762-014-0620-1

503   [49]   Vargas, V. H., Paveglio, R. R., Pauletto, P. de S., Salau, N. P. G., & Dotto, L. G. ,2020,

504   Sisal fiber as an alternative and cost-effective adsorbent for the removal of methylene

505   blue and reactive black 5 dyes from aqueous solutions. *Chemical Engineering*

506   *Communications*, **207**, 523–536. https://doi.org/10.1080/00986445.2019.1605362

507   [50]   Manikandan, V., Vanitha, A., Ranjith Kumar, E., & Chandrasekaran, J., 2017, Effect of

508   In substitution on structural, dielectric and magnetic properties of $CuFe_2O_4$

509   nanoparticles. *Journal of Magnetism and Magnetic Materials* **432**, 477–483.

510   https://doi.org/10.1016/j.jmmm.2017.02.030

511   [51]   Achary, L. S. K., Kumar, A., Barik, B., Nayak, P. S., Tripathy, N., Kar, J. P., & Dash,

512   P., 2018, Reduced graphene oxide-$CuFe_2O_4$ nanocomposite: A highly sensitive room

513   temperature NH3 gas sensor. *Sensors and Actuators, B: Chemical* **272**, 100–109.

514   https://doi.org/10.1016/j.snb.2018.05.093

515   [52]   Rouhani, S., Rostami, A., Salimi, A., & Pourshiani, O., 2018, Graphene

516   oxide/CuFe2O4 nanocomposite as a novel scaffold for the immobilization of laccase

517   and its application as a recyclable nanobiocatalyst for the green synthesis of

518   arylsulfonyl benzenediols. *Biochemical Engineering Journal* **133**, 1–11.

519   https://doi.org/10.1016/j.bej.2018.01.004

520 [53] Córdova, B. M., Santa Cruz, J. P., Ocampo, T. V. M., Huamani-Palomino, R. G., &

521   Baena-Moncada, A. M., 2020, Simultaneous adsorption of a ternary mixture of brilliant

522   green, rhodamine B and methyl orange as artificial wastewater onto biochar from cocoa

523   pod husk waste. Quantification of dyes using the derivative spectrophotometry method.

524   *New Journal of Chemistry*, **44**, 8303–8316. https://doi.org/10.1039/d0nj00916d

525 [54] Liang, T., Wang, F., Liang, L., Liu, M., & Sun, J., 2016, Magnetically separable

526   nitrogen-doped mesoporous carbon with high adsorption capacity. *Journal of Materials*

527   *Science* **51**, 3868–3879. https://doi.org/10.1007/s10853-015-9706-5

528 [55] Hoang, L. P., Van, H. T., Hang Nguyen, T. T., Nguyen, V. Q., & Thang, P. Q., 2020,

529   Coconut shell activated carbon/$CoFe_2O_4$ composite for the removal of rhodamine B

530   from aqueous solution. *Journal of Chemistry*. https://doi.org/10.1155/2020/9187960

531 [56] Rouhi, M., Lakouraj, M. M., Tashakkorian, H., & Hasantabar, V., 2019, Novel carbon

532   based bioactive nanocomposites of aniline/indole copolymer for removal of cationic

533   dyes from aqueous solution: Kinetics and isotherms. *New Journal of Chemistry* **43**,

534   2400–2410. https://doi.org/10.1039/c8nj02924e

535 [57] Aljeboree, A. M., Alshirifi, A. N., & Alkaim, A. F., 2017, Kinetics and equilibrium

536   study for the adsorption of textile dyes on coconut shell activated carbon. *Arabian*

537   *Journal of Chemistry* **10**, S3381–S3393. https://doi.org/10.1016/j.arabjc.2014.01.020

538 [58] Jarrah, A., & Farhadi, S., 2020, Preparation and characterization of novel

539   polyoxometalate/$CoFe_2O_4$/metal-organic framework magnetic core-shell

540   nanocomposites for the rapid removal of organic dyes from water. *RSC Advances* **10**

541   39881–39893. https://doi.org/10.1039/d0ra04603e

542 [59] Banerjee, S., & Chattopadhyaya, M. C., 2017, Adsorption characteristics for the

543   removal of a toxic dye, tartrazine from aqueous solutions by a low cost agricultural by-

544   product. *Arabian Journal of Chemistry* **10**, S1629–S1638.

545   https://doi.org/10.1016/j.arabjc.2013.06.005

546   [60]   Njikam, E., & Schiewer, S., 2012, Optimization and kinetic modeling of cadmium

547   desorption from citrus peels: A process for biosorbent regeneration. *Journal of*

548   *Hazardous Materials* **213–214**, 242–248.

549   https://doi.org/10.1016/j.jhazmat.2012.01.084

550   [61]   El Messaoudi, N., Dbik, A., El Khomri, M., Sabour, A., Bentahar, S., & Lacherai, A.

551   ,2017, Date stones of Phoenix dactylifera and jujube shells of Ziziphus lotus as

552   potential biosorbents for anionic dye removal. *International Journal of*

553   *Phytoremediation* **19**, 1047–1052. https://doi.org/10.1080/15226514.2017.1319331

554   [62]   Lima, E. C., Sher, F., Guleria, A., Saeb, M. R., Anastopoulos, I., Tran, H. N., &

555   Hosseini-Bandegharaei, A., 2020, Is one performing the treatment data of adsorption

556   kinetics correctly? *Journal of Environmental Chemical Engineering* **9**, 104813.

557   https://doi.org/10.1016/j.jece.2020.104813

558   [63]   El Khomri, M., El Messaoudi, N., Dbik, A., Bentahar, S., & Lacherai, A., 2020,

559   Efficient adsorbent derived from Argania Spinosa for the adsorption of cationic dye:

560   Kinetics, mechanism, isotherm and thermodynamic study. *Surfaces and Interfaces* **20**,

561   100601. https://doi.org/10.1016/j.surfin.2020.100601

562   [64]   Khan, M. A., Al Othman, Z. A., Kumar, M., Ola, M. S., & Siddique, M. R., 2020,

563   Biosorption potential assessment of modified pistachio shell waste for methylene blue:

564   thermodynamics and kinetics study. *Desalination and Water Treatment* **56**, 146–160.

565   https://doi.org/10.1080/19443994.2014.934728

566   [65]   Tahir, N., Bhatti, H. N., Iqbal, M., & Noreen, S., 2017, Biopolymers composites with

567   peanut hull waste biomass and application for Crystal Violet adsorption. *International*

568   *Journal of Biological Macromolecules*, **94**, 210–220.

569   https://doi.org/10.1016/j.ijbiomac.2016.10.013

570 [66] Tiwari, D. P., Singh, S. K., & Sharma, N., 2015, Sorption of methylene blue on treated

571   agricultural adsorbents: equilibrium and kinetic studies. *Applied Water Science* **5**, 81–

572   88. https://doi.org/10.1007/s13201-014-0171-0

573 [67] Bentahar, S., Dbik, A., Khomri, M. E., El Messaoudi, N., & Lacherai, A. , 2018,

574   Removal of a cationic dye from aqueous solution by natural clay. *Groundwater for*

575   *Sustainable Development* **6**, 255–262. https://doi.org/10.1016/j.gsd.2018.02.002

576 [68] Jerold, M., Vasantharaj, K., Joseph, D., & Sivasubramanian, V., 2017, Fabrication of

577   hybrid biosorbent nanoscale zero-valent iron-Sargassum swartzii biocomposite for the

578   removal of crystal violet from aqueous solution. *International Journal of*

579   *Phytoremediation* **19**, 214–224. https://doi.org/10.1080/15226514.2016.1207607

580 [69] Mittal, H., & Mishra, S. B., 2014, Gum ghatti and Fe_3O_4 magnetic nanoparticles based

581   nanocomposites for the effective adsorption of rhodamine B. *Carbohydrate Polymers*

582   **101**, 1255–1264. https://doi.org/10.1016/j.carbpol.2013.09.045

583 [70] Chao, Y., Pang, J., Bai, Y., Wu, P., Luo, J., He, J.,Zhu, W., 2020, Graphene-like

584       $BN@SiO_2$ nanocomposites as efficient sorbents for solid-phase extraction of

585   Rhodamine B and Rhodamine 6G from food samples. *Food Chemistry* **320**, 126666.

586   https://doi.org/10.1016/j.foodchem.2020.126666

587 [71] Mohammed, M. I., & Baytak, S., 2019, Synthesis of Bentonite–Carbon Nanotube

588   Nanocomposite and Its Adsorption of Rhodamine Dye From Water. *Arabian Journal*

589   *for Science and Engineering* **41**, 4775–4785. https://doi.org/10.1007/s13369-016-2190-

590   7

591 [72] Srivastava, V., & Choubey, A. K., 2020, Study of adsorption of anionic dyes over

592   biofabricated crystalline α-MnO_2 nanoparticles. *Environmental Science and Pollution*

593   *Research*, 1–15. https://doi.org/10.1007/s11356-020-11622-1

594 [73] Pei, Y., Wang, M., Tian, D., Xu, X., & Yuan, L., 2015, Synthesis of core-shell

SiO$_2$@MgO with flower like morphology for removal of crystal violet in water. *Journal of Colloid and Interface Science*, **453**, 194–201. https://doi.org/10.1016/j.jcis.2015.05.003

[74] Lima, E. C., Hosseini-Bandegharaei, A., Moreno-Piraján, J. C., & Anastopoulos, I., 2019, A critical review of the estimation of the thermodynamic parameters on adsorption equilibria. Wrong use of equilibrium constant in the Van't Hoof equation for calculation of thermodynamic parameters of adsorption. *Journal of Molecular Liquids* **273**, 425–434. https://doi.org/10.1016/j.molliq.2018.10.048

[75] Wu, Y., Luo, H., Wang, H., Wang, C., Zhang, J., & Zhang, Z., 2013, Adsorption of hexavalent chromium from aqueous solutions by graphene modified with cetyltrimethylammonium bromide. *Journal of Colloid and Interface Science* **394**, 183–191. https://doi.org/10.1016/j.jcis.2012.11.049

[76] Laksaci, H., Khelifi, A., Belhamdi, B., & Trari, M., 2019, The use of prepared activated carbon as adsorbent for the removal of orange G from aqueous solution. *Microchemical Journal* **145**, 908–913. https://doi.org/10.1016/j.microc.2018.12.001

[77] Liu, J., Wang, Y., Fang, Y., Mwamulima, T., Song, S., & Peng, C., 2018, Removal of crystal violet and methylene blue from aqueous solutions using the fly ash-based adsorbent material-supported zero-valent iron. *Journal of Molecular Liquids* **250**, 468–476. https://doi.org/10.1016/j.molliq.2017.12.003

[78] El Messaoudi, N., El Khomri, M., Dbik, A., Bentahar, S., & Lacherai, A., 2019, Selective and competitive removal of dyes from binary and ternary systems in aqueous solutions by pretreated jujube shell (Ziziphus lotus). *Journal of Dispersion Science and Technology* **38**, 1168–1174. https://doi.org/10.1080/01932691.2016.1228070

[79] Khorasani, A. C., & Shojaosadati, S. A., 2019, Magnetic pectin-Chlorella vulgaris biosorbent for the adsorption of dyes. *Journal of Environmental Chemical Engineering*

620 **7**, 103062. https://doi.org/10.1016/j.jece.2019.103062

621 [80] Tuzen, M., Sarı, A., & Saleh, T. A., 2018, Response surface optimization, kinetic and

622   thermodynamic studies for effective removal of rhodamine B by magnetic AC/CeO2

623   nanocomposite. *Journal of Environmental Management* **206**, 170–177.

624   https://doi.org/10.1016/j.jenvman.2017.10.016

625 [81] Cui, W., Kang, X., Zhang, X., & Cui, X. ,2019, Gel-like ZnO/Zr-MOF(bpy)

626   nanocomposite for highly efficient adsorption of Rhodamine B dye from aqueous

627   solution. *Journal of Physics and Chemistry of Solids* **134**, 165–175.

628   https://doi.org/10.1016/j.jpcs.2019.06.004

629 [82] Tran, T. Van, Phan, T. Q. T., Nguyen, D. T. C., Nguyen, T. T., Nguyen, D. H., Vo, D.

630   V. N., Nguyen, T. D., 2020, Recyclable Fe3O4@C nanocomposite as potential

631   adsorbent for a wide range of organic dyes and simulated hospital effluents.

632   *Environmental Technology and Innovation* **20**, 101122.

633   https://doi.org/10.1016/j.eti.2020.101122

634 [83] Hu, C., Grant, D., Hou, X., & Xu, F., 2020, High rhodamine B and methyl orange

635   removal performance of graphene oxide/carbon nanotube nanostructures. *Materials*

636   *Today: Proceedings* **34**, 184–193. https://doi.org/10.1016/j.matpr.2020.02.711

637 [84] Vidya, J., John Bosco, A., Haribaaskar, K., & Balamurugan, P., 2019,Polyaniline -

638   BiVO4 nanocomposite as an efficient adsorbent for the removal of methyl orange from

639   aqueous solution. *Materials Science in Semiconductor Processing* **103**, 104645.

640   https://doi.org/10.1016/j.mssp.2019.104645

641 [85] Raza, S., Yong, X., Raza, M., & Deng, J., 2018, Synthesis of biomass trans-anethole

642   based magnetic hollow polymer particles and their applications as renewable adsorbent.

643   *Chemical Engineering Journal* **352**, 20–28. https://doi.org/10.1016/j.cej.2018.06.185

644 [86] Ahmad, A., Razali, M. H., Mamat, M., Mehamod, F. S. B., & Anuar Mat Amin, K.,

645   2017, Adsorption of methyl orange by synthesized and functionalized-CNTs with 3-

646   aminopropyltriethoxysilane loaded TiO2 nanocomposites. *Chemosphere* **168,** 474–482.

647   https://doi.org/10.1016/j.chemosphere.2016.11.028

648   [87] Hu, X., Yan, L., Wang, Y., & Xu, M., 2020, Freeze-thaw as a route to build

649   manageable polysaccharide cryogel for deep cleaning of crystal violet. *Chemical*

650   *Engineering Journal* **396**, 125354. https://doi.org/10.1016/j.cej.2020.125354

651